


# Direction-dependent elastic properties and phononic behavior of PMMA/BaTiO<sub>3</sub> nanocomposite thin films

Cite as: J. Chem. Phys. **146**, 203325 (2017); <https://doi.org/10.1063/1.4978675>

Submitted: 05 December 2016 . Accepted: 28 February 2017 . Published Online: 23 March 2017

E. Alonso-Redondo, A. Gueddida, H. Huesmann, O. El Abouti, W. Tremel , E. H. El Boudouti, B. Djafari-Rouhani, and G. Fytas



View Online



Export Citation



CrossMark

## ARTICLES YOU MAY BE INTERESTED IN

[Band structure of cavity-type hypersonic phononic crystals fabricated by femtosecond laser-induced two-photon polymerization](#)

Applied Physics Letters **108**, 201901 (2016); <https://doi.org/10.1063/1.4949013>

[Surface transport mechanisms in molecular glasses probed by the exposure of nanoparticles](#)

The Journal of Chemical Physics **146**, 203324 (2017); <https://doi.org/10.1063/1.4978667>

[Focus: Structure and dynamics of the interfacial layer in polymer nanocomposites with attractive interactions](#)

The Journal of Chemical Physics **146**, 203201 (2017); <https://doi.org/10.1063/1.4978504>



# Direction-dependent elastic properties and phononic behavior of PMMA/BaTiO<sub>3</sub> nanocomposite thin films

E. Alonso-Redondo,<sup>1,a)</sup> A. Gueddida,<sup>2,3</sup> H. Huesmann,<sup>4</sup> O. El Abouti,<sup>3</sup> W. Tremel,<sup>4</sup>  
 E. H. El Boudouti,<sup>3</sup> B. Djafari-Rouhani,<sup>2</sup> and G. Fytas<sup>1,a)</sup>

<sup>1</sup>Max Planck Institute for Polymer Research, Ackermannweg 10, 55128 Mainz, Germany

<sup>2</sup>Institut d'Electronique, de Microelectronique et de Nanotechnologie (IEMN), UMR-CNRS 8520, UFR de Physique, Université de Lille 1, 59655 Villeneuve d'Ascq, France

<sup>3</sup>LPMR, Département de Physique, Faculté des Sciences, Université Mohamed I, 60000 Oujda, Morocco

<sup>4</sup>Department of Inorganic Chemistry, Johannes Gutenberg University, Duesbergweg 10-14, 55128 Mainz, Germany

(Received 5 December 2016; accepted 28 February 2017; published online 23 March 2017)

Determination of the anisotropic mechanical properties of nanostructured hybrid films is of great importance to improve fabrication and to enable reliable utility. Here, we employ spontaneous Brillouin light spectroscopy to record the phononic dispersion relation along the two symmetry directions in a supported PMMA (poly(methylmethacrylate))-BaTiO<sub>3</sub> hybrid superlattice (SL) with a lattice constant of about 140 nm. Several dispersive elastic modes are resolved for in-plane wave propagation, whereas along the periodicity direction the SL opens a wide propagation stop band for hypersonic phonons and near UV photons both centered at about 280 nm. A thorough theoretical analysis based on the finite element method quantitatively captures the band diagrams along the two main symmetry directions, helps identify the large density mismatch effect on the unexpectedly low sound phase velocity, and reveals significant anisotropy of the SL elastic tensor. Phonon propagation is a sensitive index of the structure, density, and the mechanical moduli of nanocomposite films. *Published by AIP Publishing.* [<http://dx.doi.org/10.1063/1.4978675>]

## I. INTRODUCTION

The destructive interference of elastic waves phenomenon has been used for the design of customized materials that are deaf in a certain range of frequencies. Those materials are termed phononic crystals, and they exhibit a bandgap of forbidden frequencies ( $f \sim \pi/a$ ) that commensurate their lattice constant ( $a$ ).<sup>1,2</sup> In nanocomposites, the bandgap—which is in the hypersonic range (GHz)—occurs at characteristic lengths comparable to the visible light (VIS) wavelengths.<sup>3</sup> This is of particular interest for potential applications involving the interaction of acoustic and visible waves, e.g., cavity mirrors,<sup>4</sup> optomechanical resonators,<sup>5,6</sup> and sensors.<sup>7,8</sup> Due to the vector character of elastic waves and the multiple parameters involved in their propagation, one-dimensional (1D) nanocomposites facilitate the fundamental studies of phononic crystals. This was realized already prior to the theoretical prediction of phononic bandgaps<sup>9,10</sup> by reporting in 1979 selective transmission of elastic waves in superlattices (SLs), i.e., phonon filtering by dielectric Bragg mirrors.<sup>11</sup> The SL platform allows the manipulation of elastic wave propagation in periodic structures. For example, longitudinal phonons folded<sup>12</sup> to the Brillouin zone (BZ) and confined acoustic vibrations<sup>13</sup> in semiconductor SLs have been observed by Raman scattering.<sup>12,14,15</sup> This earlier work has stimulated further studies in search of phononic bandgaps<sup>16–18</sup> establishing the concepts of unidirectional

bandgap in the case of 1D hypersonic phononic crystals.<sup>19</sup> Several applications benefit from the SL designs such as coherent phonon generation,<sup>20</sup> acoustic diodes,<sup>21</sup> and decrease of heat conductivity.<sup>22</sup>

The use of polymers expands the performance possibilities of nanocomposites, in opposition to rigid crystals, due to their elastic versatility, an inexpensive fabrication, and their general biocompatibility.<sup>23,24</sup> The combination of polymers with inorganic materials opens new routes for the generation of quality and functional hybrid phononic structures. Hybrid (organic-inorganic) superlattices (SLs) can be prepared over large areas and are excellent coatings for multiple applications in photonics such as selective mirrors.<sup>25,26</sup> Through the phononic behavior of SLs, knowledge on the elastic properties—necessary for an optimal performance—can be obtained.<sup>27</sup> Silica and poly(methylmethacrylate) (SiO<sub>2</sub>-PMMA) SLs, studied by non-destructive Brillouin spectroscopy (BLS), have advanced our understanding of sound propagation that opens new pathways to tunable hybrid periodic films. For example, the architecture of finite SLs with controlled defects allows the engineering of the bandgap region through the interaction of surface and cavity vibration modes.<sup>28,29</sup> In the case of spin-coated SiO<sub>2</sub>-PMMA SLs, the bandgap width of the hybrid SL has been limited by the porosity of the inorganic layer (to  $\Delta f/f_g \approx 30\%$ , here  $f_g$  is the mid-frequency of the gap). This limitation on the elastic impedance contrast has been overcome by the fabrication of polycarbonate (PC) and tungsten (W) SLs by pulsed laser deposition; the PC/W interface roughness is significantly low and the structure exhibits a broad ( $\Delta f/f_g \approx 70\%$ )

<sup>a)</sup>Authors to whom correspondence should be addressed. Electronic addresses: [fyas@mpip-mainz.mpg.de](mailto:fyas@mpip-mainz.mpg.de) and [alonso@mpip-mainz.mpg.de](mailto:alonso@mpip-mainz.mpg.de).

bandgap.<sup>30</sup> The disadvantages of pulsed-laser deposited SLs over spin-coated SLs relate to the complex sample preparation which involves controlled vacuum and temperature conditions. The replacement of the porous SiO<sub>2</sub> phase by a heavier phase, such as barium titanate (BaTiO<sub>3</sub>), in spin-coated SLs is expected to have an impact on the bandgap width.

Determination of the mechanical properties of nanostructured soft materials and their composites in a quantitative manner is of great importance to improve the fidelity in their fabrication and to enable subsequent reliable utility. While the mechanical properties of bulk materials are well-established, those of thin and patterned soft matter are subject to variations inherent to the fabrication and subsequent aging.<sup>31,32</sup> Mechanical properties and the stability of nanostructured materials are of importance for a wide range of applications that comprise coatings, microelectronics, photonics, nano-electromechanical systems, and biomedical technologies. As many coatings exhibit substantial anisotropy<sup>33,34</sup> of structure and properties, direct access to both in-plane and out-of-plane elastic constants becomes necessary. A non-destructive characterization of the mechanical properties of films is therefore of key importance in advancing microlithography and coating-based technologies. BLS is a powerful technique for a detailed study of the direction-dependent elastic wave propagation in transparent nanostructures.<sup>34</sup> In the case of SL films, the presence of symmetry renders the elastic wave propagation outside the bandgap region (along the periodicity direction) and normal to the periodicity direction inherently anisotropic and hence a unique assessment of direction dependent elastic constants of the film is required for a complete mechanical characterization at nanoscale.<sup>29</sup>

Here, we present a fast and compact procedure to fabricate high impedance hybrid SLs. We make use of the spin-coating technique to prepare PMMA and BaTiO<sub>3</sub> SLs and nanocomposite films at room conditions (1 atm and 25 °C). The large mismatch between the densities of PMMA (1190 kg/m<sup>3</sup>) and BaTiO<sub>3</sub> (6020 kg/m<sup>3</sup>) is the key parameter in the phononic behavior of the SL in the in-plane and out-of-plane directions. In the in-plane direction, multiple elastic excitations are recorded due to the thin character of the film. In the out-of-plane (periodicity) direction, we record the photonic and phononic behaviors. The dual bandgap is not sacrificed despite the interfacial roughness inherent to the spin-coating fabrication. We independently characterize films of nanoparticle composite (PMMA and BaTiO<sub>3</sub>) that mimic the porous BaTiO<sub>3</sub> layer in the SL.

## II. METHODS AND CHARACTERIZATION

The hybrid superlattice film was prepared from PMMA and BaTiO<sub>3</sub> nanoparticles by the spin-coating technique. The BaTiO<sub>3</sub> perovskite nanoparticles are prepared by a hydrothermal synthesis using barium (Ba) and titanium isopropoxide (*Sigma Aldrich*).<sup>35</sup> In order to determine their morphology, nanoparticles are drop-coated on a carbon-coated copper grid and measured with a transmission electron microscope (TEM, *JEOL 1400*). Nanoparticles size is  $7 \pm 1$  nm and their shape is approximately spherical (Fig. 1(a)). For the fabrication of the SL, layers of PMMA (2.5 wt. % in toluene) and BaTiO<sub>3</sub> nanoparticles (20 g/l in ethanol) are alternatively spin-coated onto a clean glass substrate (5000 rpm, 20 s). After each layer, the sample is dried at 100 °C for 15 min. The microstructure of the SL is characterized by scanning electron microscope (SEM, *Leo Gemini 1530*). The average lattice constant is  $a = 141 \pm 15$  nm, and hence the total thickness of the 10 bilayer superlattice film is  $h = 1410$  nm (Fig. 1(b)).

In order to obtain the refractive index necessary to calculate the  $q(n)$  out-of-plane, the photonic UV-VIS spectrum is measured with a spectrometer (*Cary 5G Varian*) at normal incidence. The UV-VIS spectrum (Fig. 2) displays a minimum of transmittance at  $\lambda_B = 430$  nm. From the Bragg-Snell law  $\lambda_B = 2n_{eff}a$  we estimate the effective refractive index of the SL as  $n_{eff} = 1.53$ . The width of the gap is given by  $\Delta\lambda = \frac{4\lambda_0}{\pi} \sin^{-1} \left( \frac{n_{BaTiO_3} - n_{PMMA}}{n_{BaTiO_3} + n_{PMMA}} \right) \approx 50$  nm.<sup>36</sup> These results are in good agreement with the shaded region in Fig. 2, associated to the minimum in transmission. The transmission does not reach unity because of the finite size of the structure (10 bilayers) and the absorption in the BaTiO<sub>3</sub> layers; this quantity has been taken into account in the simulation spectra (blue line in Fig. 2) by adding a small imaginary part to the refractive index of BaTiO<sub>3</sub>. The simulation of the photonic spectrum has been done using an analytic Green function method,<sup>37</sup> while the same result can be found by simulation using the finite element method (FEM) based on *Comsol Multiphysics* software.

The phonon dispersion relation (frequency vs. wave vector) of the superlattice is experimentally characterized by Brillouin light scattering (BLS) spectroscopy along the layers (in-plane) and across the layers (out-of-plane). BLS is based on the elasto-optic interaction of the incident light with thermally activated phonons that causes a Brillouin double shift ( $\pm\omega$ ) in the spectrum of homogeneous media. The spectrum of nanostructured media consists of several Brillouin shifts corresponding to the different probed modes. The magnitude of the probing wave vector  $\mathbf{q} = \mathbf{k}_s - \mathbf{k}_i$  (where  $\mathbf{k}_i$  ( $\mathbf{k}_s$ ) is the

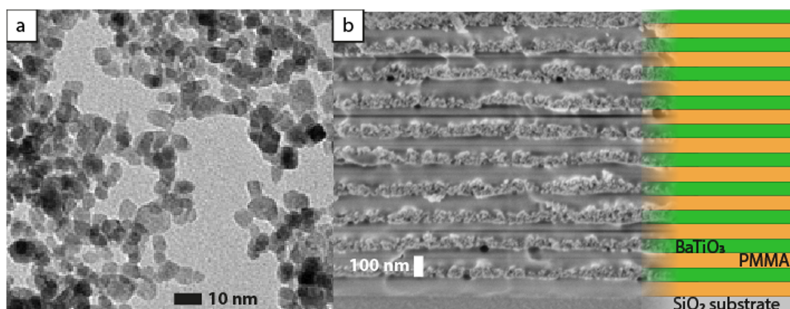


FIG. 1. (a) TEM micrograph of BaTiO<sub>3</sub> particles dispersed in a TEM grid. (b) Cross section SEM micrograph of the multilayer BaTiO<sub>3</sub>-PMMA superlattice.

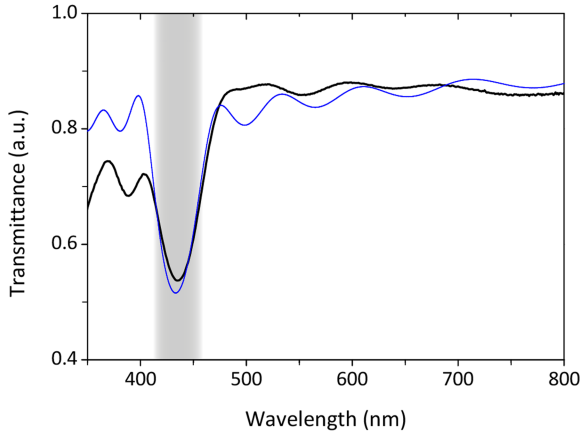


FIG. 2. UV-VIS photonic transmittance of the BaTiO<sub>3</sub>-PMMA superlattice, experimental (black) and theoretical (blue). The shaded region denotes the bandgap.

incident (scattered) light wave vector) depends on the scattering geometry. In transmission geometry,  $\mathbf{q}$  lies in the substrate plane and its magnitude is  $q_{\parallel} = 4\pi/\lambda \sin(\theta/2)$ , where  $\theta$  is the angle between  $\mathbf{k}_i$  and  $\mathbf{k}_s$ , and  $\lambda = 532$  nm is the wavelength of the laser beam. Note the independency of  $q_{\parallel}$  from the refractive index. In reflection geometry,  $\mathbf{q}$  is perpendicular to the substrate plane and its magnitude  $q_{\perp}(n_{eff})$  depends on the effective refractive index of the sample.

The dispersion relation and the displacement fields of the PMMA/BaTiO<sub>3</sub> SL modes are obtained by solving the elasticity equations of motion by using *Comsol Multiphysics* software based on the finite element method (FEM), while they can be also obtained by the analytic Green function approach.<sup>28</sup> The governing equations of motion which describe the propagation of the hypersonic phonons in such structure are given by

$$-\rho\omega^2\mathbf{u} = \nabla\sigma, \quad (1)$$

where  $\rho$  is the mass density,  $\omega(=2\pi f)$  is the pulsation,  $\mathbf{u}$  is the displacement vector, and  $\sigma$  is the elastic stress tensor. The proposed structure consists of 20 alternating PMMA and BaTiO<sub>3</sub> layers deposited along the  $y$  direction on a semi-infinite glass substrate. The structure is infinite along the  $x$  and  $z$  directions. Along the periodicity direction, the dispersion curves of an infinite superlattice are obtained by considering one unit cell of a PMMA/BaTiO<sub>3</sub> bilayer and applying the periodic boundary conditions.<sup>38</sup> The knowledge of the dispersion relation allows us to calculate the BLS spectra. The main elasto-optic interaction mechanism in transparent materials is based on the photon-phonon interaction that results in the change of the dielectric permittivity tensor  $\delta\epsilon_{ij}$  at each point of the sample, due to its modulation by the acoustic wave, according to the proportionality of  $\delta\epsilon_{ij}$  to the elastic strain  $S_{kl}$ ,  $\delta\epsilon_{ij} = P_{ijkl} S_{kl}$ . Here  $P_{ijkl}$  are the components of the photoelastic tensor. A simple approach of the Brillouin intensity is then given by

$$I = |E_j^s|^2 \propto \left| \frac{1}{\omega} \iint_{unit.cell} e^{iqr} \sum_{ikl} P_{ijkl} S_{kl} E_i^l dS \right|^2, \quad (2)$$

where  $E_j^s$  is the  $j$  component of the scattered electric field,  $E_i^l$  is the  $i$  component of the electric field from the probing laser, and  $\mathbf{q}$  is the wave vector. In isotropic materials, there are only two independent photoelastic coefficients, namely,  $P_{11}$

(= $P_{1111}$ ) and  $P_{12}$  (= $P_{1122}$ ). In our problem, the scattered electric field  $E^s$  and the incident electric field  $E^l$  are both polarized in the  $z$  direction, either the acoustic wave propagation is in-plane or out-of-plane. Then, Equation (2) becomes as follows. For in-plane propagation:

$$I(\omega, q_{\parallel}) \propto \left| \sum_{\alpha} \frac{1}{\omega} \iint e^{iq_{\parallel}x} P_{12}^{\alpha} \left( \frac{\partial u_x}{\partial x} + \frac{\partial u_y}{\partial y} \right) E^0 dS \right|^2. \quad (3)$$

For out-of-plane propagation:

$$I(\omega, q_{\perp}) \propto \left| \sum_{\alpha} \frac{1}{\omega} \iint e^{iq_{\perp}y} P_{12}^{\alpha} \left( \frac{\partial u_y}{\partial y} \right) E^0 dS \right|^2, \quad (4)$$

where  $q_{\parallel}$  and  $q_{\perp}$  are, respectively, the wave vector for propagation parallel and perpendicular to the layers,  $u_x$  and  $u_y$  are the components of the displacement field associated with the elastic wave,  $E^0$  is the incident electric field, and  $P_{12}^{\alpha}$  is the photoelastic coefficient in medium  $\alpha$ .

### III. IN-PLANE PROPAGATION

Experimental polarized BLS spectra at different scattering wave vectors  $q_{\parallel}$  (in-plane and normal to the periodicity direction), and at room temperature, are displayed in Fig. 3(a) for an almost symmetric supported BaTiO<sub>3</sub>/PMMA SL. There is more than a single acoustic peak and hence the BLS spectra are represented by up-to three Lorentzian lines. The obtained frequencies at the peak position of the Lorentzian line shapes vs.  $q_{\parallel}$  are shown in the dispersion plot of Fig. 3(b) (open diamonds). The deviation from the linear acoustic behavior is better shown in the plot of the effective phase sound velocity  $c_i$  ( $c_{\parallel} = 2\pi f_i/q_{\parallel}$ ) of the  $i$ th-mode as a function of the reduced quantity  $hq_{\parallel}$  (Fig. 3(c)), where  $h$  is the total thickness of the SL film.<sup>39,40</sup> Above about  $hq_{\parallel} > 10$ , the phonon wavelength ( $2\pi/q_{\parallel}$ ) becomes smaller than the thickness, and the effective medium longitudinal sound velocity,  $c_{\parallel} = 2620 \pm 13$  m/s is reached. This  $c_{\parallel}$  value in the SL is surprisingly low, being even lower than in the soft PMMA sublayer ( $c_{PMMA} = 2800$  m/s, Table I).

An explanation of such low effective sound velocity in the SL could be the association of the observed modes at high  $hq_{\parallel}$  values (Fig. 3(c)) to guided-Sezawa type modes. In the case of a slow supported film on a fast substrate, the Sezawa modes—which are guided modes in the supported film—have been more often studied in the vicinity of transverse velocity of the film<sup>45</sup> and are therefore mainly of transverse character. In Fig. 3(c), these kind of Sezawa modes are those situated on the dispersion curves which go below 2620 m/s (visible only at low  $hq_{\parallel}$ , i.e., wavelength larger than thickness). The observed mode which asymptotically goes to 2620 m/s (Figs. 3(b) and 3(c)) is of longitudinal character and is identified with the guided longitudinal mode of the supported film. The computed field maps of modes propagating in the supported film at high  $hq_{\parallel}$  ( $=17$ ) values clearly reveal predominant localization of the longitudinal displacement field within the film (Fig. S1 of the [supplementary material](#)). Longitudinal guided modes have, for instance, been observed in a ZnSe supported film<sup>46</sup> and a GaN-AlN supported bilayer.<sup>47</sup> The longitudinal guided modes at high  $hq_{\parallel}$  are therefore not related to the interface between the SL and the substrate and can exist even in



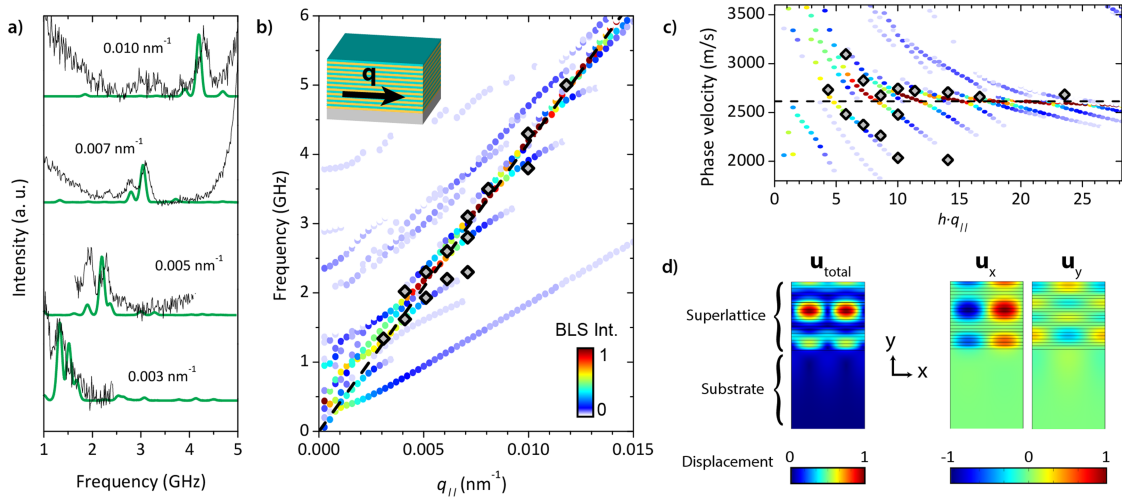


FIG. 3. In-plane propagation. (a) Experimental (black) and theoretical (green) BLS spectra at the anti-Stokes side. (b) Dispersion relation along the layers. The black diamonds are for the experimental dispersion, while the colored dots are for the theoretical dispersion relation; the color denotes the BLS intensity (white color represents zero intensity). (c) Phase velocity vs.  $h \cdot q_{||}$  ( $h$  is the thickness of the film). The dashed lines in (b) and (c) mark the sound line of the SL. (d) Displacement field (total and along the  $x$  and  $y$  directions) of a wave propagating along  $x$  at  $q_{||} = 0.0051 \text{ nm}^{-1}$  and  $f = 2.20 \text{ GHz}$ , in a cross section of the SL one wavelength long.

free-standing films (Fig. S2 of the [supplementary material](#)). Therefore, the low effective sound velocity in the SL cannot be rationalized with a description based on the Sezawa modes.

Prior to the discussion of this unexpected finding, first we discuss on other characteristic features of the in-plane elastic modes in Fig. 3(c). In contrast to the present SL, no dispersive acoustic modes were discernible in a similar hybrid spincoated  $\text{SiO}_2/\text{PMMA}$ ; the reader is referred to Schneider *et al.*<sup>28</sup> Instead, a single longitudinal acoustic phonon was observed corresponding to the effective medium sound velocity, higher than in bulk PMMA. The main difference between the two SLs is the density of the inorganic phase of the SLs, higher in the  $\text{BaTiO}_3/\text{PMMA}$  SL ( $\rho_{\text{BaTiO}_3} = 3300 \text{ kg/m}^3$  vs.  $\rho_{\text{SiO}_2} = 1420 \text{ kg/m}^3$ ), that can quantitatively affect the dispersion of the film guided modes. In the case of  $\text{SiO}_2/\text{PMMA}$  SL, the dispersion is shifted to lower  $q_{||}$  compared to the  $\text{BaTiO}_3/\text{PMMA}$  SL and renders the resolution of the elastic modes difficult. This notion was further corroborated by the observation of predominantly longitudinal guided mode in a spincoated  $\text{TiO}_2/\text{PMMA}$  SL with denser  $\text{TiO}_2$  sublayers ( $\rho_{\text{TiO}_2} = 1900 \text{ kg/m}^3$ ) than the  $\text{SiO}_2$  layers of the  $\text{SiO}_2/\text{PMMA}$  SL.<sup>41</sup> Hence for similar sound velocities of the hard layers (same

soft PMMA layer), the in-plane phonon dispersion depends sensitively on their density.

The in-plane acoustic excitations are guided modes in the SL as indicated in the space distribution of the displacement field (Fig. 3(d)). The elastic energy is mainly associated with the longitudinal ( $u_x$ ) motion of the acoustic wave and the exact vertical location depends on the probed modes as shown in Figs. 4(a) and 4(c) at a given  $q_{||}$  ( $=0.0051 \text{ nm}^{-1}$ ) for two different modes. Along the periodicity direction ( $y$ ), the square modulus of the displacement field for the two modes is relatively low in support of their longitudinal character. In order to address the importance of the periodicity, we have theoretically examined the in-plane guided modes of a homogeneous film with the effective elastic parameters and thickness as in the corresponding SL.<sup>42</sup> The behavior in both film and SL is found to be quantitatively the same as shown in the elastic energy distribution in Figs. 4(b) and 4(d) for two modes with very similar frequencies. This result clearly supports the idea that the guided mode pattern is robust to the disorder of the nanocomposite films.

We turn now to the unexpectedly low effective medium longitudinal sound velocity  $c_{||}$  ( $= 2620 \pm 13 \text{ m/s}$ ) in the  $\text{BaTiO}_3/\text{PMMA}$  SL. Given the unexpected effective  $c_{||}$  (Fig. 4), we examined its value in  $\text{BaTiO}_3/\text{PMMA}$  nanocomposites with different volume fractions of the hard component. The films prepared by spin-coating of mixed solution were much thicker ( $5 \mu\text{m}$ ) than the SL, so that one effective medium longitudinal acoustic mode is recorded by BLS. Figure 5 shows the volume fraction dependence of the experimentally and theoretically obtained  $c_{||}$  in  $\text{BaTiO}_3$ -PMMA nanocomposites at  $23^\circ\text{C}$ . Remarkably,  $c_{||}$  remains lower than its value in the soft PMMA for all examined blend compositions, and even revealing an abrupt drop above  $\phi_{\text{BaTiO}_3} = 0.2$ . To theoretically estimate  $c_{||}$ , we consider the mixture of  $\text{BaTiO}_3$  particles in PMMA as a periodic structure with a face-centered cubic (FCC) lattice. The effective velocities of this three-dimensional phononic crystal are calculated in the long wavelength limit with elastic

TABLE I. Physical quantities of the  $\text{BaTiO}_3$ -PMMA superlattice constituents and substrate used in the calculations.

| Parameter <sup>a</sup>     | $\text{BaTiO}_3$ layer <sup>b</sup> | PMMA layer  | $\text{SiO}_2$ substrate |
|----------------------------|-------------------------------------|-------------|--------------------------|
| $\rho$ ( $\text{kg/m}^3$ ) | 3300                                | 1190        | 2200                     |
| $c_L$ (m/s)                | 2570                                | 2800        | 5660                     |
| $c_T$ (m/s)                | 1400                                | 1400        | 3250                     |
| $d$ (nm)                   | $67 \pm 10$                         | $74 \pm 12$ | 1 mm                     |
| $n$                        | 1.58                                | 1.49        | 1.50                     |

<sup>a</sup>Density ( $\rho$ ), longitudinal sound velocity ( $c_L$ ), transverse sound velocity ( $c_T$ ), thickness ( $d$ ), and refractive index ( $n$ ).

<sup>b</sup>Porous.

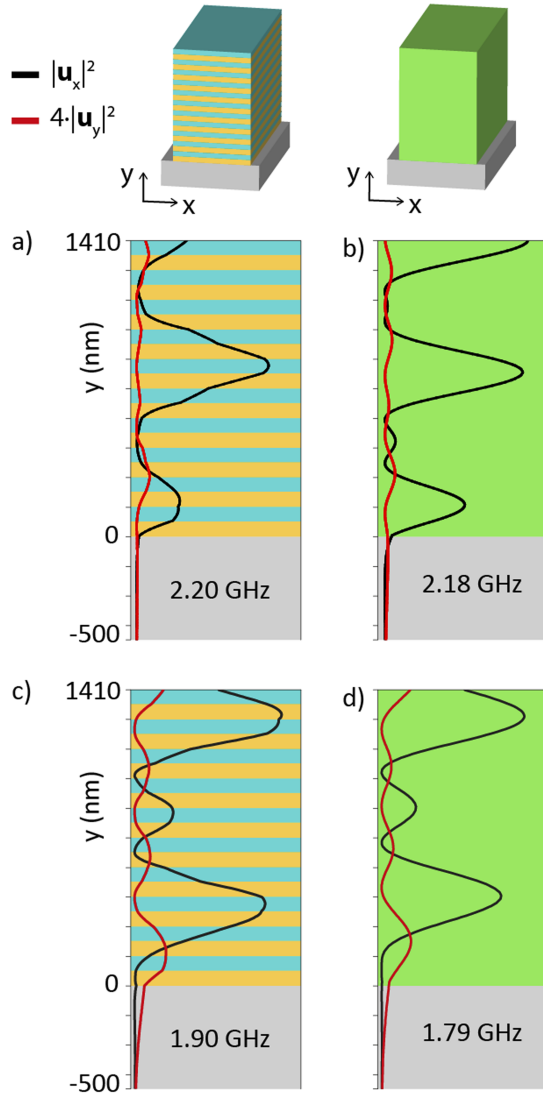


FIG. 4. Square of the displacement field of an observed mode in-plane at  $0.0051 \text{ nm}^{-1}$  in the superlattice ((a) and (c)) and in the homogeneous layer ((b) and (d)). The grey shaded region is the substrate.

parameters of the bulk  $\text{BaTiO}_3$  ( $\rho_{\text{BaTiO}_3} = 6012 \text{ kg/m}^3$ ,  $c_{L,\text{BaTiO}_3} = 5910 \text{ m/s}$ ,  $c_{T,\text{BaTiO}_3} = 3050 \text{ m/s}$ )<sup>43</sup> and PMMA (Table I). The decrease of  $c_{//}(\phi_{\text{BaTiO}_3})$  is only qualitatively predicted by the theoretical calculations (along the [100] and [111] directions), as the minimum of the experimental  $c_{//}(\phi_{\text{BaTiO}_3})$  is much shallower and appears at lower  $\text{BaTiO}_3$  composition. The composition dependence of  $c_{//}$  in Fig. 5 clearly shows the failure of the commonly used Wood's effective medium equation which is essentially an interpolation between the two component elastic moduli.<sup>44</sup> A hypothetical model to explain the sharp drop in  $c_{//}$  of the film would be to introduce some voids into the previous unit cell of the periodic structure. Among many possibilities, we show in Fig. 5 an example in which 9 voids are introduced along the four diagonals of the cube in the following way: one at the center of the cube and the 8 others at the 8 positions equivalent to  $(a/4, a/4, a/4)$ , where  $a$  is the unit cell size (inset of Fig. 5). The effective velocities along the [100] and [111] directions are calculated for 3 different radii  $R_v$  of the void spheres. In this calculation, if  $R_v$  increases such that the void spheres overlap with the  $\text{BaTiO}_3$

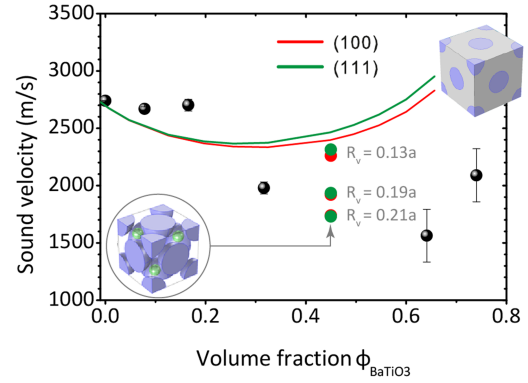


FIG. 5. Effective longitudinal sound velocities of  $\text{BaTiO}_3$  and PMMA composite films as a function of volume fraction of  $\text{BaTiO}_3$ . The black dots are for the experiment and the color lines for the simulation of a FCC lattice of  $\text{BaTiO}_3$  spheres in PMMA, along the two main crystallographic directions. The green and red dots at  $\phi = 0.45$  denote the effective velocity in the same FCC lattice, with spherical voids of three different radii  $R_v$  (the voids are represented as green spheres in the fcc unit cell of the inset).

nanoparticles, we assume that the overlapping space remains filled with  $\text{BaTiO}_3$ . The result in Fig. 5 shows a sharp decrease of the effective velocity when increasing  $R_v$ . Further decrease of the velocity can even be obtained by inserting additional holes around the previous ones. Therefore, an explanation of the very low effective velocity of sound may be the presence of voids, although our very simple model that corresponds to a particular periodic structure does not take into account the effect of disorder.

#### IV. OUT-OF-PLANE PROPAGATION

Along the SL periodicity direction, we have recorded the BLS spectra for  $q_{\perp}$ , normal to the film, near the reduced Brillouin zone ( $q_{\text{BZ}} \approx \pi/a$ ).<sup>2</sup> The BLS spectra of Fig. 6(a) show a double peak structure, corresponding to a phononic interference-based (Bragg) bandgap, as displayed in the dispersion relation in Fig. 6(b). The experimental spectra can be theoretically represented using the component sound velocities and densities in Table I, and the same photoelastic coefficients ( $P_{\text{BaTiO}_3} = P_{\text{PMMA}}$ ) used for the calculation of the in-plane BLS spectra (Fig. 3(a)). The choice of the photoelastic coefficients is based on the best representation of the BLS spectra out-of-plane and is justified by the strong infiltration of the  $\text{BaTiO}_3$  layers. The experimental frequencies are captured in the dispersion relation by Rytov's equation of an infinite SL<sup>38</sup> and the parameters of Table I. We recall that for the determination of  $q_{\perp}$  we used the refractive index  $n_{\text{eff}} = 1.53$  as estimated from the photonic gap (Fig. 2). The frequency separation of the two branches is the highest among the known SL fabricated by spin-coating leading to a large bandgap width (5.5 GHz) in the dispersion of Fig. 6(b). The elastic energy near the BZ is predominately located in the soft PMMA phase for the upper frequency branch as inferred from the displacement field of Fig. 6(c). For the lower frequency branch, the elastic energy would be located in the hard  $\text{BaTiO}_3$  phase (not shown here).<sup>41</sup>

The effective medium sound velocity,  $c_{\perp} = 2390 \text{ m/s}$ , was obtained at low  $q_{\perp}$  ( $a q_{\perp} < 1$ ) envisaging the SL as a single uniform layer with longitudinal modulus,  $M_{\perp} = \rho c_{\perp}^2$ ,

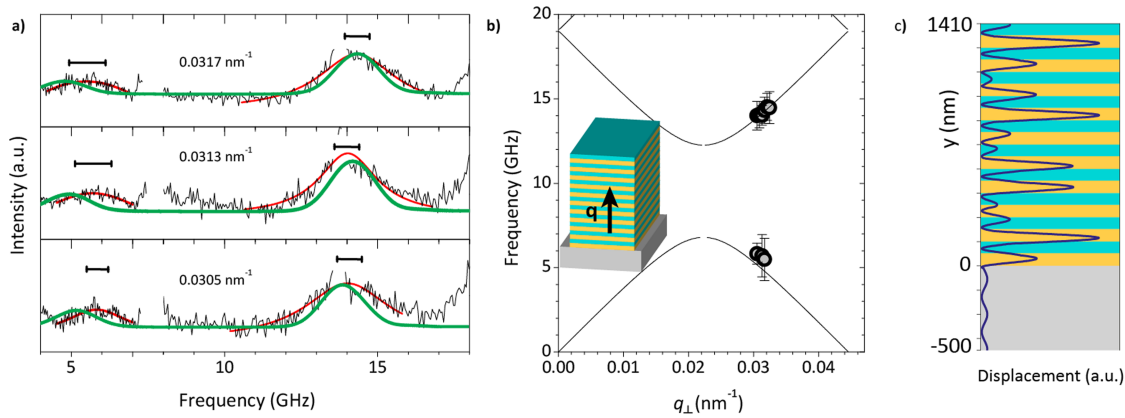


FIG. 6. Out-of-plane propagation. (a) Experimental (black) and theoretical (green) BLS spectra. The experimental spectra have been represented by a sum of Lorentzian shapes (red lines). The cut in the experimental spectra is due to the two free spectral ranges used. (b) Dispersion relation across the layers. The black dots are for the experimental dispersion, while the solid lines are for the theoretical dispersion curves of an infinite SL. (c) Displacement field at  $q_{\perp} = 0.0323 \text{ nm}^{-1}$  and  $f = 14.65 \text{ GHz}$ .

where  $\rho$  ( $=2190 \text{ kg/m}^3$ ) is the mean density. The value of  $c_{\perp}$  can be also obtained from Wood's law,<sup>43</sup>  $M^{-1} = \varphi/M_{\text{BaTiO}_3} + (1 - \varphi)/M_{\text{PMMA}}$ , where the moduli of the constituent layers,  $M_{\text{BaTiO}_3} = 21.8 \text{ GPa}$ ,  $M_{\text{PMMA}} = 9.3 \text{ GPa}$ , are estimated from the densities and sound velocities of Table I. The effective medium sound velocities,  $c_{\parallel}$ ,  $c_{\perp}$ , along the two symmetry directions are different, with  $c_{\perp}$  being about 8% lower. Assuming isotropic density, the effective in-plane elastic constant ( $C_{11} = M$ ) is about 15% higher than the out-of-plane ( $C_{33}$ ) component revealing anisotropy of the elastic tensor of SLs. The anisotropy is larger than that in spin-coated  $\text{SiO}_2/\text{PMMA}$  and  $\text{TiO}_2/\text{PMMA}$  SLs.<sup>28,41</sup>

Hypersonic SLs are photonic structures in the visible with very similar phonon and photon wavelength stop bands. In fact, the phononic bandgap is for  $\Lambda$  ( $\approx 2\pi/0.0225 \text{ nm}^{-1}$ ) about 280 nm (Fig. 6(b)), while the photonic gap occurs at  $\lambda$  ( $\approx 432/1.53$ )  $\approx 282 \text{ nm}$  (Fig. 2).

## V. CONCLUSIONS

We have studied the elastic wave propagation in supported 10 bilayer  $\text{BaTiO}_3/\text{PMMA}$  SL film along and normal (out-of-plane and in-plane) to the periodicity direction using BLS and theoretical analysis. The effective refractive index of the SL was obtained from the minimum UV-VIS photonic transmittance and found to be lower than in bulk  $\text{BaTiO}_3$  due to the PMMA infiltration of the  $\text{BaTiO}_3$  layer in the SL. This inevitable infiltration effect of the spin-coating fabrication is responsible for the decrease of the effective medium sound velocity even below the value in the soft PMMA layer. The isotropic wave propagation in the constituent layers becomes direction dependent with not only distinct dispersion (frequency vs. wave vector) relations but also effective medium sound velocities. Full representation of the BLS experiment (dispersion curves and intensities) using FEM calculations is necessary to identify the in-plane dispersive modes, capture the characteristics of the unidirectional bandgap, and rationalize the low and direction dependent effective medium sound velocities.

For the finite SL thickness, in-plane propagation reveals up to three dispersive modes with mixed polarization which

are well described using the density and elastic constants of the PMMA and the PMMA infiltrated  $\text{BaTiO}_3$  layer. The resolution of these modes, absent in other  $\text{SiO}_2/\text{PMMA}$  SLs, is facilitated by the large density contrast that also leads to the reduction of the effective medium sound velocity (softening of the elastic modulus) of the SL. Notably, the dispersive modes are insensitive to the SL layered structure and depend only on the used spatial resolution,  $hq_{\parallel}$ , given by the film thickness ( $h$ ) and the in-plane wave vector ( $q_{\parallel}$ ). The anticipated phononic bandgap along the periodicity direction with  $\approx 0.6$  bandgap width to mid-gap frequency ratio is one of the largest among the known hybrid SLs due to the large density contrast. Concurrently, the SL acts also as phoxonic 1D crystal with dual bandgaps for both photons and phonons with mid gap wavelength  $\approx 280 \text{ nm}$ . Although a spin-coating technique provides a facile fabrication of SLs with a large range of materials, the unavoidable softening of the hard layer limits further increase of the stop bandwidth compared with other fabrication techniques, e.g., pulsed laser deposition. For the effective medium elastic modulus ( $C_{33}$ ) along the periodicity assumes a lower ( $\sim 15\%$ ) value than the in-plane value ( $C_{11}$ ).

## SUPPLEMENTARY MATERIAL

See [supplementary material](#) for the displacement fields of a supported and a free standing SL, along with their dispersion diagram.

## ACKNOWLEDGMENTS

We thank A. Reuss for the spincoating of the nanocomposite films. The work was supported by ERC SmartPhon No. 694977.

<sup>1</sup>F. R. Montero de Espinosa, E. Jiménez, and M. Torres, *Phys. Rev. Lett.* **80**(6), 1208–1211 (1998).

<sup>2</sup>J. O. Vasseur, P. A. Deymier, G. Frantzikonis, G. Hong, B. Djafari-Rouhani, and L. Dobrzynski, *J. Phys.: Condens. Matter* **10**(27), 6051–6064 (1998).

<sup>3</sup>W. Cheng, J. J. Wang, U. Jonas, G. Fytas, and N. Stefanou, *Nat. Mater.* **5**(10), 830–836 (2006).

<sup>4</sup>A. Fainstein, N. D. Lanzillotti-Kimura, B. Jusserand, and B. Perrin, *Phys. Rev. Lett.* **110**(3), 037403 (2013).

- <sup>5</sup>T. Czerniuk, C. Brüggemann, J. Tepper, S. Brodbeck, C. Schneider, M. Kamp, S. Höfling, B. A. Glavin, D. R. Yakovlev, A. V. Akimov, and M. Bayer, *Nat. Commun.* **5**, 4038 (2014).
- <sup>6</sup>J. Chan, T. P. Alegre, A. H. Safavi-Naeini, J. T. Hill, A. Krause, S. Groblacher, M. Aspelmeyer, and O. Painter, *Nature* **478**(7367), 89–92 (2011).
- <sup>7</sup>F. Vollmer and S. Arnold, *Nat. Methods* **5**(7), 591–596 (2008).
- <sup>8</sup>J. Botsis, L. Humbert, F. Colpo, and P. Giaccari, *Opt. Lasers Eng.* **43**(3-5), 491–510 (2005).
- <sup>9</sup>M. Kushwaha, P. Halevi, L. Dobrzynski, and B. Djafari-Rouhani, *Phys. Rev. Lett.* **71**(13), 2022–2025 (1993).
- <sup>10</sup>M. Sigalas and E. N. Economou, *Solid State Commun.* **86**(3), 141–143 (1993).
- <sup>11</sup>V. Narayanamurti, H. L. Störmer, M. A. Chin, A. C. Gossard, and W. Wiegmann, *Phys. Rev. Lett.* **43**(27), 2012–2016 (1979).
- <sup>12</sup>C. Colvard, R. Merlin, M. V. Klein, and A. C. Gossard, *Phys. Rev. Lett.* **45**(4), 298–301 (1980).
- <sup>13</sup>M. Trigo, A. Bruchhausen, A. Fainstein, B. Jusserand, and V. Thierry-Mieg, *Phys. Rev. Lett.* **89**(22), 227402 (2002).
- <sup>14</sup>P. X. Zhang, D. J. Lockwood, H. J. Labbé, and J. M. Baribeau, *Phys. Rev. B* **46**(15), 9881–9884 (1992).
- <sup>15</sup>N. D. Lanzillotti Kimura, A. Fainstein, and B. Jusserand, *Phys. Rev. B* **71**(4), 041305(R) (2005).
- <sup>16</sup>L. C. Parsons and G. T. Andrews, *Appl. Phys. Lett.* **95**(24), 241909 (2009).
- <sup>17</sup>P. M. Walker, J. S. Sharp, A. V. Akimov, and A. J. Kent, *Appl. Phys. Lett.* **97**(7), 073106 (2010).
- <sup>18</sup>G. N. Aliev, B. Goller, D. Kovalev, and P. A. Snow, *Appl. Phys. Lett.* **96**(12), 124101 (2010).
- <sup>19</sup>N. Gomopoulos, D. Maschke, C. Y. Koh, E. L. Thomas, W. Tremel, H. J. Butt, and G. Fytas, *Nano Lett.* **10**(3), 980–984 (2010).
- <sup>20</sup>R. P. Beardsley, A. V. Akimov, M. Henini, and A. J. Kent, *Phys. Rev. Lett.* **104**(8), 085501 (2010).
- <sup>21</sup>B. Liang, X. S. Guo, J. Tu, D. Zhang, and J. C. Cheng, *Nat. Mater.* **9**(12), 989–992 (2010).
- <sup>22</sup>Y. K. Koh, Y. Cao, D. G. Cahill, and D. Jena, *Adv. Funct. Mater.* **19**(4), 610–615 (2009).
- <sup>23</sup>M. C. Chiappelli, A. Ribbe, A. W. Hauser, and R. C. Hayward, *Sens. Actuators, B* **208**, 85–89 (2015).
- <sup>24</sup>A. Retolaza, J. Martínez-Perdiguero, S. Merino, M. Morales-Vidal, P. G. Boj, J. A. Quintana, J. M. Villalvilla, and M. A. Díaz-García, *Sens. Actuators, B* **223**, 261–265 (2016).
- <sup>25</sup>M. Akihiro, F. Kenji, T. Tetsuro, A. Kikuo, O. Hisashi, and T. Keiji, *Chem. Lett.* **40**(10), 1138–1139 (2011).
- <sup>26</sup>S.-J. Jeon, M. C. Chiappelli, and R. C. Hayward, *Adv. Funct. Mater.* **26**(5), 722–728 (2016).
- <sup>27</sup>G. Saini, T. Pezeril, D. H. Torchinsky, J. Yoon, S. E. Kooi, E. L. Thomas, and K. A. Nelson, *J. Mater. Res.* **22**(03), 719–723 (2006).
- <sup>28</sup>D. Schneider, F. Liaqat, E. H. El Boudouti, Y. El Hassouani, B. Djafari-Rouhani, W. Tremel, H. J. Butt, and G. Fytas, *Nano Lett.* **12**(6), 3101–3108 (2012).
- <sup>29</sup>D. Schneider, F. Liaqat, E. El Boudouti, O. El Abouti, W. Tremel, H. J. Butt, B. Djafari-Rouhani, and G. Fytas, *Phys. Rev. Lett.* **111**(16), 164301 (2013).
- <sup>30</sup>F. Döring, H. Ulrichs, S. Pagel, M. Müller, M. Mansurova, M. Müller, C. Eberl, T. Erichsen, D. Huebner, P. Vana, K. Mann, M. Münzenberg, and H.-U. Krebs, *New J. Phys.* **18**(9), 092002 (2016).
- <sup>31</sup>M. P. Stoykovich, H. B. Cao, K. Yoshimoto, L. E. Ocola, and P. F. Nealey, *Adv. Mater.* **15**(14), 1180 (2003).
- <sup>32</sup>R. Hartschuh, Y. Ding, J. H. Roh, A. Kisliuk, A. P. Sokolov, C. L. Soles, R. L. Jones, T. J. Hu, W. L. Wu, and A. P. Mahorowala, *J. Polym. Sci., Part B: Polym. Phys.* **42**, 1106–1113 (2004).
- <sup>33</sup>P. Akcora, H. Liu, S. K. Kumar, J. Moll, Y. Li, B. C. Benicewicz, L. S. Schadler, D. Acehan, A. Z. Panagiotopoulos, V. Pryamitsyn, V. Ganesan, J. Ilavsky, P. Thiyagarajan, R. H. Colby, and J. F. Douglas, *Nat. Mater.* **8**(4), 354–359 (2009).
- <sup>34</sup>P. Voudouris, J. Choi, N. Gomopoulos, R. Sainidou, H. C. Dong, K. Matyjaszewski, M. R. Bockstaller, and G. Fytas, *ACS Nano* **5**(7), 5746–5754 (2011).
- <sup>35</sup>L. Huang, Z. Jia, I. Kyriassis, and S. O'Brien, *Adv. Funct. Mater.* **20**(4), 554–560 (2010).
- <sup>36</sup>P. Yeh, *Optical Waves in Layered Media* (Wiley, 2005).
- <sup>37</sup>M. L. H. Lahlouiti, A. Akjouj, B. Djafari-Rouhani, L. Dobrzynski, M. Hamouchi, E. H. El Boudouti, and A. Nougouai, *J. Opt. Soc. Am. A* **16**(7), 1703–1714 (1999).
- <sup>38</sup>S. M. Rytov: *Akust. Zh.* **2**, 71 (1956) [*Sov. Phys.-Acoust.* **2**, 68 (1956)].
- <sup>39</sup>W. Cheng, R. Sainidou, P. Burgardt, N. Stefanou, A. Kiyanova, M. Efremov, G. Fytas, and P. F. Nealey, *Macromolecules* **40**(20), 7283–7290 (2007).
- <sup>40</sup>J. A. Rogers, A. A. Maznev, M. J. Bane, and K. A. Nelson, *Annu. Rev. Mater. Sci.* **30**, 117–157 (2000).
- <sup>41</sup>E. Alonso-Redondo, H. Huesmann, E.-H. El Boudouti, W. Tremel, B. Djafari-Rouhani, H.-J. Butt, and G. Fytas, *ACS Appl. Mater. Interfaces* **7**, 12488–12495 (2015).
- <sup>42</sup>B. Djafari-Rouhani and J. Sapriel, *Phys. Rev. B* **34**(10), 7114–7117 (1986).
- <sup>43</sup>Z. Li, S. K. Chan, M. H. Grimsditch, and E. S. Zouboulis, *J. Appl. Phys.* **70**(12), 7327 (1991).
- <sup>44</sup>A. B. Wood, *Textbook of Sound* (Macmillan, 1930).
- <sup>45</sup>T. Wittkowski, G. Distler, K. Jung, B. Hillebrands, and J. D. Comins, *Phys. Rev. B* **69**(20), 205401 (2004).
- <sup>46</sup>B. Hillebrands, S. Lee, G. I. Stegeman, H. Cheng, J. E. Potts, F. Nizzoli, *Phys. Rev. Lett.* **60**, 832–835 (1988).
- <sup>47</sup>M. Chirita, R. Sooryakumar, R. Venugopal, J. Wan, and M. R. Melloch, *Phys. Rev. B* **63**, 205302 (2001).